Reversible–irreversible plasticity transition in twinned copper nanopillars

J.A. Brown, N.M. Ghoniem [*]

Mechanical and Aerospace Engineering, University of California, Los Angeles, CA 90095, USA

Abstract

Through computer simulations, we show that plasticity in twinned copper nanopillars can be either reversible or irreversible depending on the applied stress state. Copper nanopillars, containing twinned crystals, are subjected to both compression and tension, and the ratio of the resolved shear (σ_R) to the normal stress (σ_N), R, is adjusted through variation of the orientation of the twin boundary plane with respect to the loading axis. It is found that the yield locus on the σ_R–σ_N plane for twinned nanopillars is asymmetric with respect to the sign of R. For a 9 nm diameter copper nanopillar under compression, plastic deformation can be totally reversed when σ_R is in the range $0.5 \leqslant \sigma_R \leqslant 1$ GPa, with a corresponding increase in the compressive normal stress, up to ≈ 2.5 GPa. It is shown that these conditions are achieved for axial strains <3.3%, and that the transition to plastic irreversibility takes place at larger strains or normal stresses. The mechanism responsible for the plastic reversible–irreversible transition is shown to be a competition between the nucleation of Shockley partial dislocations at the nanopillar surface for irreversible plasticity vs. twinning dislocations for reversible plasticity. Furthermore, the speed of Shockley partials at twin boundaries is subsonic when there is either tension or compression acting on the twin boundary, and slightly supersonic when only shear is applied.
© 2009 Acta Materialia Inc. Published by Elsevier Ltd. All rights reserved.

Keywords: Copper; MD simulations; Twin boundary; Nanopillars; Plasticity

1. Introduction

While the elastic deformation of solid crystals is completely determined by a few elastic constants, plasticity is the result of creation and motion of lattice defects requiring many degrees of freedom. At the atomic level, plastic deformation is facilitated by several basic mechanisms involving grain boundary sliding, diffusional creep, slip through dislocation motion and twin boundary migration. It is generally associated with the irreversible deformation of solid crystals, because processes such as atomic diffusion and defect nucleation require an energy barrier, and, as such, atomic motion cannot be reversed because part of the energy used to cross such barriers is irreversibly dissipated. However, in situations where deformation is accompanied by a phase transformation (e.g. growth of a martensitic phase), large shape change can be realized through the reversible motion of phase boundaries [1]. The ability to control the geometry, and hence the corresponding mechanical and physical properties of nanoscale materials and devices, is of great interest in many applications, such as in microelectromechanical devices with small-scale contacts, the fabrication and use of nanowires in logic and memory circuits, and in structural reinforcements of composite materials [2].

Recently, there has been a great deal of interest in exploring the plastic deformation characteristics of nanoscale materials, such as nanograined, nanotwinned and nanopillar metals [3–9]. By controlling the size of grains and producing nanocrystalline metals whose grain sizes are of the order of 100 nm or less, strength levels exceeding 4–5 times those with grain sizes on the micron level can be easily achieved. Recent experiments have also shown that the high density

[*] Corresponding author.
E-mail address: ghoniem@ucla.edu (N.M. Ghoniem).

of nanoscale growth twins in fine-grained copper dramatically elevates the strength while providing considerable tensile ductility [3,4]. In addition to nanocrystalline and nanotwinned materials, several experimental techniques have recently been developed to fabricate metallic and silicon cylinders with nanoscale dimensions, known as nanopillars. Experimental techniques such as scanning tunneling microscopy [10], electron-beam lithography [11], "scratch" lithography [12], cluster-beam deposition of metallic etch masks [13], laser irradiation [14] and colloidal gold natural lithography [15] have been recently advanced.

The mechanical deformation of these nanopillars beyond the elastic regime shows unusual characteristics that are not observed in bulk materials. Deformation of single-crystal nanopillars has been explored using molecular dynamics (MD) simulation by Rabkin et al. who demonstrated that the primary yielding mechanism under uniaxial compression is by nucleation of Shockley partial dislocations from the surface [16]. Additionally, a variety of conditions has been shown to influence the yielding behavior of metallic single-crystal nanopillars. Among these are the strain rate [9,17,18], the initial shape of the sample [19], the temperature [17] as well as the size scale of the pillar [20,21]. However, when considering polycrystalline nanopillars, the interaction of grain boundaries and dislocations produces a yet more complex picture. Deformation mechanisms in nanopillars containing multiple grains can be accommodated by either grain boundary migration, grain boundary sliding, motion of existing dislocations and nucleation of new dislocations from surfaces and grain boundaries. The preferred mechanism can depend on a variety of conditions ranging from the orientation and direction of the crystallography relative to the deformation, the availability of slip planes or the lattice energies of the respective defects. This was later confirmed by Zepeda-Ruiz et al. using large-scale simulations comparable to those of experiment on single-crystal Au nanopillars with diameters of 10–20 nm under uniaxial compression [20]. Additionally, they observed highly non-uniform stress states leading to yielding behavior that was highly dependent upon surface facets and orientation.

Other unique aspects of nanoscale material deformation have also been recently shown. For example, the computer simulation work of Afanasyev et al. showed significant hardening of gold nanopillars under compression due to the interaction of dislocations that had been nucleated from the surface with perpendicular twin boundaries [22]. Gall et al. examined the yield strength under tensile loading of gold nanowires of varying widths, down to the subnanometer level [21], and observed an increase in the strength of nanowires due to a surface-stress-induced change in the stable structure of the nanowires. Park and Zimmerman [23] and Ma et al. [17] also performed MD simulations of gold nanowires under tensile loading, and examined the effects of the strain rate and wire size on its plastic deformation. Their work demonstrated the importance of the stacking fault and surface energies in accurately capturing nanoscale deformation mechanisms. Likewise, Zhu et al.

used both simulation and high-resolution transmission electron microscopy observations in order to examine the strain-rate sensitivity of nanotwinned copper [8]. They described this rate sensitivity in terms of the interaction of dislocations with interfaces, and demonstrated that slip-transfer reactions mediated by twin boundary interactions are the rate-controlling mechanisms. Since the surface-to-volume ratio is very high in nanoscale materials, particularly nanowires and nanopillars, the influence of free surfaces on plasticity has been the subject of numerous recent investigations as well. The effects of free surfaces on yielding was studied by Diao et al. [24] for gold nanowires, and by Li and Ghoniem [25] for twinned copper. The specific mechanism of dislocation nucleation from the free surface was determined via MD simulations by Zhu et al. [18], who developed a framework to describe the probabilistic nature of dislocation nucleation from surfaces. Dislocation nucleation conditions were also investigated by Tschopp and McDowell, who studied bulk single-crystal copper under uniaxial loading, and examined how homogeneous nucleation of partial dislocations changes as a function of crystallographic orientation [26]. Most recently, Dutta et al. have proposed a model of lattice resistance to the motion of a dislocation within a nanosized system, where the dislocation velocity is enhanced as a result of the proximity to the surface [27].

The objective of the present work is to explore the conditions that control two important modes of plastic deformation in copper nanopillars: dislocation nucleation from the surface and twin boundary migration. The main aim here is to show that a transition from reversible to irreversible plastic flow can be induced in axially loaded nanopillars, and that a tension–compression asymmetry is inherent in plastically deforming nanopillars. These two aspects—namely the reversible–irreversible plasticity transition and the tension–compression asymmetry—will be traced to fundamental atomic mechanisms through MD computer simulations. In the next section, we discuss details of computer simulations, followed by a presentation of simulation results in Section 3, where we discuss the deformation modes, the tension–compression asymmetry and the atomic mechanisms responsible for the observed behavior. Finally, we give conclusions of the present study in Section 4.

2. Computational methods

Atomic interactions in all MD simulations here were modeled using an embedded atom method (EAM) potential for copper that accurately reproduces the cohesive energy, point defect energies, phonon frequencies and other properties [28]. The potential gives twin boundary and intrinsic stacking fault energies, as well as elastic constants that are in agreement with experiments [28], which are key properties for accurate simulation of dislocation behavior. The EAM potential gives direct access to an average mechanical stress tensor on an ensemble of atoms, $\langle \boldsymbol{\sigma} \rangle$, given by [29,30]:

$$\langle \boldsymbol{\sigma} \rangle = \frac{1}{V} \sum_{\alpha} \sum_{\beta \neq \alpha} \left[\frac{1}{2} \Phi'_{\alpha\beta}(r_{\alpha\beta}) + F'(\langle \rho_\alpha \rangle) \rho'_\beta(r_{\alpha\beta}) \right] \frac{\boldsymbol{r}_{\alpha\beta} \otimes \boldsymbol{r}_{\alpha\beta}}{r_{\alpha\beta}},$$

$$(1)$$

where $V = \sum_\alpha \Omega_\alpha$ is the total volume of the ensemble, Ω_α the atomic volume assigned to atom α, $r_{\alpha\beta}$ is the distance between atoms α and β, connected by the vector $\boldsymbol{r}_{\alpha\beta}$, $\Phi_{\alpha\beta}$ is the pair interaction function, ρ_β is the electron density induced by atom β, $F(\langle \rho_\alpha \rangle)$ is the embedding energy of atom α and $\langle \rho_\alpha \rangle$ is the background electron density on the location of atom α. While the way the total volume is partitioned between atoms is somewhat arbitrary, the average stress does not depend on the choice of individual atomic volumes. In this work we choose Ω_α to be the equilibrium atomic volume in the perfect lattice $k^3 \Omega_0$, where Ω_0 is the atomic volume at 0 K and k^3 is a predetermined linear thermal expansion factor appropriate to the temperature at which the simulation is performed.

Once the atomic stress tensor is determined, the average traction ($\langle \boldsymbol{t} \rangle$), normal stress ($\langle \sigma_N \rangle$) and resolved shear stress ($\langle \sigma_R \rangle$) acting on an atomic plane with unit normal vector ($\boldsymbol{n}$) can be obtained as:

$$\langle \boldsymbol{t} \rangle = \langle \boldsymbol{\sigma} \rangle \cdot \boldsymbol{n}; \quad \langle \sigma_N \rangle = \langle \boldsymbol{t} \rangle \cdot \boldsymbol{n}; \quad \langle \sigma_R \rangle = \sqrt{\langle \boldsymbol{t} \rangle \cdot \langle \boldsymbol{t} \rangle - \sigma_N^2} \quad (2)$$

We will define here the shear load ratio, R, as the ratio of the resolved shear stress divided by the normal stress. It is a measure of the relative strength of the shear stress acting on the twin plane, thus $R = \langle \sigma_R \rangle / \langle \sigma_N \rangle$. An atomic simulation block is initially prepared with construction of a large orthorhombic volume of approximate dimensions $20 \times 2 \times 36$ nm, along the x, y and z directions, respectively. The y-axis was chosen to align with the axial load (compression or tension) direction, while the z-axis was chosen to lie along the $[1\,\bar{1}\,0]$ crystallographic direction, which selectively isolates the δ or γ (using Thompson's tetrahedron notation) slip planes as preferred slip systems. Then, by varying the axial load direction, the angle formed between the load axis and the slip plane normal can be controlled, resulting in prescribed stress components (normal and shear) on slip planes. The x-axis was fully determined by the choice of z- and y-axes.

A twin boundary was then constructed by performing 180° rotation of the half-grain above a selected slip plane (1 1 1) relative to the other half. For each simulation, the angle θ formed between the load axis and the twin boundary normal controls the shear load ratio, R. Each simulation block consisted of either two, four or six twin boundaries evenly spaced apart, such as to remain non-interacting with themselves, the base or the top of the simulation block. In addition to the rotation, in-phase shifts (shifts which preserved the twin symmetry), lateral to the rotation plane were also performed on the half-grains simply to keep the block as squared as possible. Finally, all atoms outside a cylinder with a diameter of 9 nm and of a height between 27 and 30 nm were removed from the simulation block, thus leaving an atomically smooth cylindrical surface behind. Fig. 1 shows a diagram of this
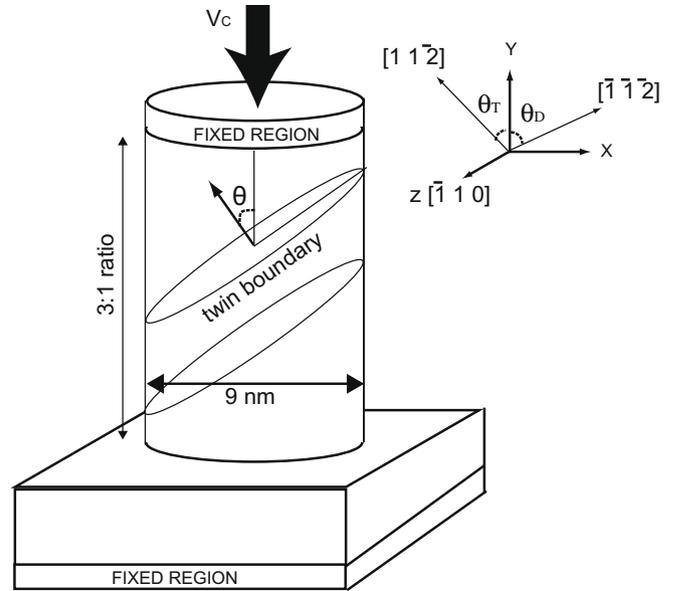

Fig. 1. Schematic of the nanopillar geometry. The two sections labeled "fixed region" are atoms which are constrained either to rigid body motion (top), or totally constrained (bottom). v_c is the rigid body velocity imposed on the upper region. The prismatic block at the bottom has periodic boundaries, while the cylindrical surface is a free boundary.

simulation block, where we show the angle θ_T between the loading axis and the $[1\,1\,\bar{2}]$ direction on the twin plane (1 1 1), and θ_D between the loading axis and the $[\bar{1}\,1\,2]$ direction on the conjugate slip plane (note that $\theta_D + \theta_T = 109.5°$, so only one angle needs to be specified).

Thin slabs of atoms at the top and bottom of the simulation block are held fixed as indicated in Fig. 1. These fixed regions are allowed to interact with their neighboring atoms, but the displacement of these atoms is constrained to be in the axial direction by the applied load at the top, and is totally constrained at the bottom. The nanopillar itself comprised free surfaces exposed to vacuum; however, the base of the nanopillar had periodic boundary conditions in the x- and z-directions creating an infinite slab on which the nanopillar was positioned. The final simulation blocks comprised of the order of 0.35 million atoms.

Prior to performing any compression or tension simulations, the simulation block was allowed to anneal for 800 ps. During this annealing process, the temperature was successively stepped up to the final simulation temperature of 500 K. As the temperature was stepped up, previously determined uniform expansions [28] were imposed on the simulation block in order to accommodate the thermal expansion as the simulation temperature was increased. By imposing this expansion, the average internal pressure was maintained at zero, and the pressure due to the free surfaces equilibrates naturally through the annealing process. All reported values and results are for a constant temperature of $T = 500$ K using an NVT ensemble. Thus, by varying the angle of the twin boundaries with respect to the compression/tension axis we are able to selectively vary the normal stress, $\langle \sigma_N \rangle$, and the critical resolved shear

stress, $\langle\sigma_R\rangle$, acting on the twin boundary. The angle θ_T controls the degree of coupling between shear displacements and twin boundary migration [31].

3. Results

3.1. Reversible–irreversible plasticity transition

Plastic deformation of twinned face-centered cubic (fcc) crystals has been shown by Li and Ghoniem to proceed via two main channels: (1) nucleation and propagation of dislocations and (2) twin boundary migration [25]. Nucleation of Shockley partial dislocations takes place at free surfaces [31], or at twin boundaries themselves [25], and, as such, will lead to irreversible plastic deformation. On the other hand, if surface dislocation nucleation is somehow prevented, and twin boundaries are subjected to sufficient shear displacement, twinning dislocations can form at these boundaries, allowing them to migrate normal to the shear plane displacement. The atomic mechanisms of this twin boundary motion "coupled" to shear deformation have recently been described within the framework of stick–slip dynamics [32,31]. Hu et al. found that the "stick" phase of the dynamics is associated with accumulated strain in the crystal, and that such strain is suddenly released by the nucleation of $1/6[11\bar{2}]$-type twinning partial dislocations [31]. In atomic layers adjacent to the twin boundary, coordinated shuffling of atoms was determined to take place immediately before dislocation nucleation. The "slip" phase of the dynamics was shown to be controlled by fast propagation of nucleated twinning partial dislocations and their spreading along the twin boundary [31].

The competing plastic yield mechanisms of surface Shockley partial dislocation nucleation vs. nucleation and propagation of twinning partial dislocations were also observed during the compression-induced grain boundary migration with coupled shear [33], or nucleation of partial dislocations from the surface [16]. The work of Afanasyev et al. demonstrated substantial strengthening of nanopillars due to the presence of nanoscale twins with twin boundaries normal to the compression axis [22], in agreement with the simulation results of Li and Ghoniem [25].

The competition between the two mechanisms is controlled by three parameters: the magnitude of applied displacement (and hence local stress tensor), the angle between the twin boundary normal and the load axis (θ), and the angle between the load axis and the $[11\bar{2}]$ direction on the twin plane, θ_T. Proper selection of the two angles, θ and θ_D (and hence θ_D) will effectively control the specific components of the stress tensor acting on twin and slip planes. Our strategy is then to utilize this specific geometry of copper (fcc) nanopillars and simple loading to determine independent values of the local normal and shear stresses on twin and slip planes. We are then able to activate both twin boundary migration without surface dislocation nucleation and surface nucleation of dislocations on conjugate slip planes. By having an even moderately low θ_T, twin

boundary migration was found to be the preferred yield mechanism resulting in an overall much softer material. However, as θ_T approaches 0° and starts to become more perpendicular to the compression axis, then the normal stress acting on the twin boundary exceeds a critical value, and the channel of plastic deformation via twin boundary migration ceases to be the dominant mode of deformation. At this point, dislocation nucleation is activated on conjugate slip planes, resulting in irreversible plasticity [22].

In traditional continuum plasticity, the yield surface is generally constructed in the stress space spanned by the three principal components (the Haigh–Westergaard space), but more conveniently projected on the two-dimensional space of principal stresses σ_1 and σ_2 (plane conditions). We select here the two components of $\langle\sigma_R\rangle$ and $\langle\sigma_N\rangle$ to show the yield condition of copper nanopillars loaded in tension (Fig. 2), and in compression (Fig. 3). In Fig. 2a, the plastic yield line is shown as a linear relationship between the local normal stress on the twin boundary and the corresponding shear stress. The insets in the figure show the inclinations of the twin boundary plane trace (solid line) and the trace of the conjugate slip plane (dashed line) with respect to the load axis. The "yield locus" shown in Fig. 2a is associated with plastic deformation of several per cent, but is reversible once a compressive load is applied. Total reversal of plastic displacement is unusual in bulk fcc metals because dislocation generation and multiplication is inevitable in bulk materials, whereas the small size of a nanopillar and the ability to precisely control the stress state at the twin boundary enables full reversal of the plastic deformation without any surface dislocation nucleation. We have shown in other publications [25,34,31] that twin boundary migration in copper is the result of nucleation and motion of twinning dislocations, and that the magnitude and direction of twin boundary motion can be controlled by the direction of shear on the twin boundary, being maximum when shear is applied along Shockley partial dislocation directions ($\langle 112\rangle$). When the local shear stress is around 0.8 GPa, and the tensile stress around 1 GPa, twin boundary motion will take place without any surface dislocations that can cause irreversibility. On the other hand, when the local shear stress is 1 GPa, the tensile stress must be close to 1.5 GPa for twin boundary motion to dictate plastic deformation, and hence these conditions result in the phenomenon of reversible plasticity. When the tensile stress becomes large (approximately above 2 GPa), the corresponding resolved shear on conjugate planes is considerable, and the imposed load displacement is plastically accommodated by the generation and propagation of dislocations from the surface in an irreversible manner. The corresponding "yield locus" for irreversible plasticity is shown in Fig. 2b.

The yield locus for twinned copper nanopillars is shown in Fig. 3, where the results of computer simulations are fitted to linear relationships between the local values of the normal stress on active slip or twin planes, and the resolved shear stress. It is clear that when the local shear stress is below
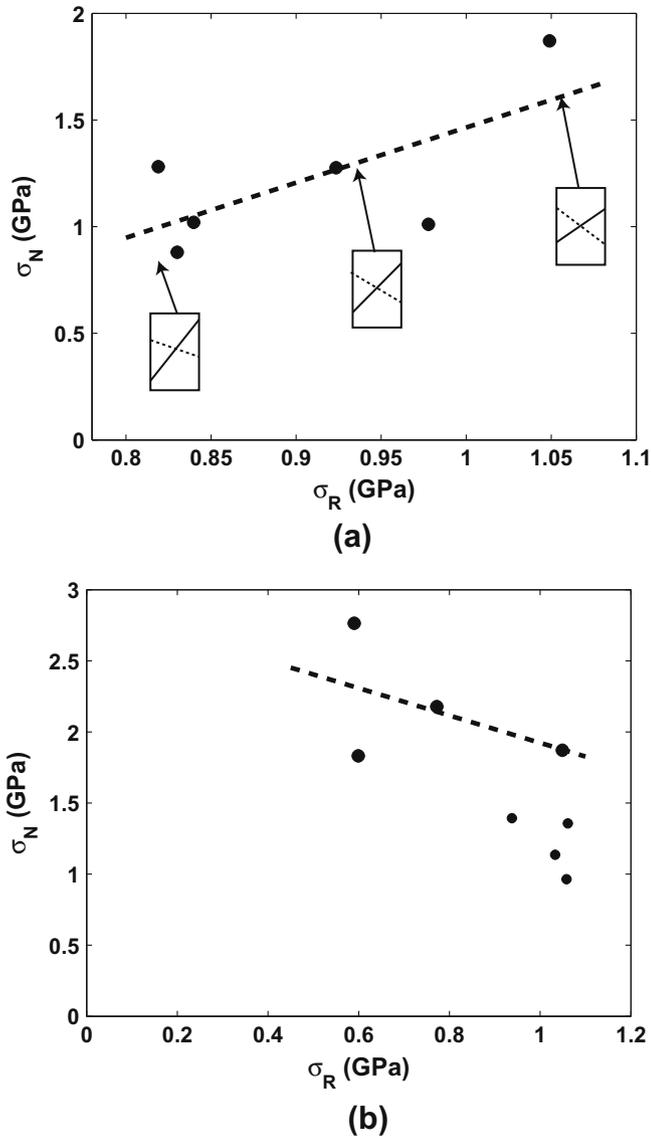
(a)

(b)

Fig. 2. "Yield locus" in the twinned nanopillar under tension shown as a linear relationship between the normal stress, $\langle \sigma_N \rangle$ and the resolved shear stress, $\langle \sigma_R \rangle$. (a) The regime of exclusively twin migration behavior (reversible plasticity) and (b) the regime of irreversible plasticity resulting from mixed behavior, where either twin migration (large black circles) or dislocation nucleation (small black circles) from the surface is indicated.

Fig. 3. The yield locus of the twinned nanopillar in compression shown as two distinct linear relationships between the normal stress, $\langle \sigma_N \rangle$ and the resolved shear stress, $\langle \sigma_R \rangle$ on active twin or slip planes. Each large black circle indicates a yielding event exclusively by twin boundary migration (reversible plasticity). Yielding by dislocation nucleation from the surface is labeled by "DN" and each yielding event is indicated by a small black circle. The white circles indicate single-crystal simulations (no nanotwins), and are included for comparison.

about 1 GPa, and the normal stress "squeezing" atoms on twin planes is very large (e.g. above ≈ 2.5 GPa), twin boundary can no longer be sustained, and another plastic deformation channel opens up in the form of dislocation nucleation from the surface. The state of plastic reversibility at local shear stresses in the range $0.5 \leqslant \langle \sigma_R \rangle \leqslant 1$ GPa can be attained with a corresponding increase in the compressive normal stress, up to ≈ 2.5 GPa. Beyond these limits, copper twinned nanopillars make a transition to a state of plastic irreversibility attained by surface dislocation nucleation and twin boundary migration.

The critical transition from reversible to irreversible plasticity is demonstrated in Fig. 4, where it is clearly shown that below a strain of about 3.3%, twinned copper
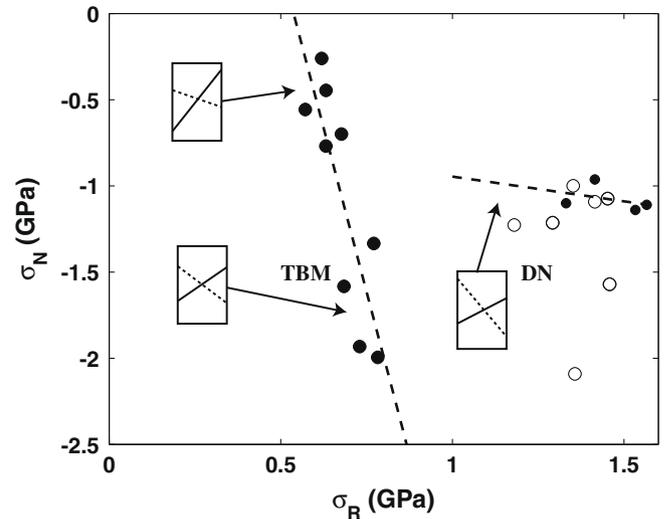
nanopillars prefer to deform plastically by twin boundary migration, and thus the deformation is reversible since it is not associated with any surface dislocations. At larger values of strain, plastic deformation becomes irreversible, as can be seen in Fig. 4. This behavior is unique to twinned nanopillars, and is not observed in bulk crystals.

3.2. Tension–compression asymmetry

In some polycrystalline metals, the yield point in tension is different from that under compression. This tension–compression asymmetry is called the Bauschinger effect in polycrystalline materials. In the present computer simulations of nanotwinned pillars, we also observe a tension–compression asymmetry reminiscent of the Bauschinger effect, although the physical mechanisms are entirely different. Fig. 5 shows the yield locus in tension and in compression for reversible plasticity controlled by twin boundary migration. Under compression, a lower value of the local shear stress is needed to initiate yield by twin boundary migration, as compared to the same conditions under tension. Twinning dislocation nucleation and motion is facilitated when the twin boundary is under compression, as compared to being under tension. However, and in both cases, a larger value of local shear is required to initiate twin boundary migration when any normal stress is additionally operating on the twin plane. The nucleation and motion of twinning dislocations on the twin boundary becomes more difficult as atoms move away from their equilibrium separation under the influence of a large compressive or tensile normal stress. We show at the end of this section that the speed of dislocation motion on twin
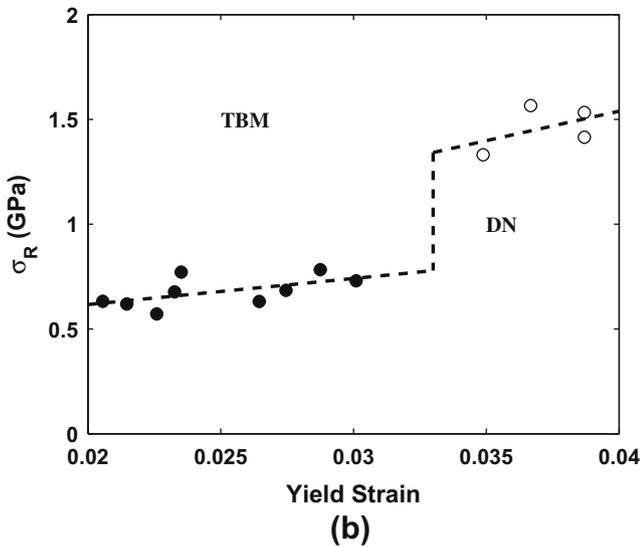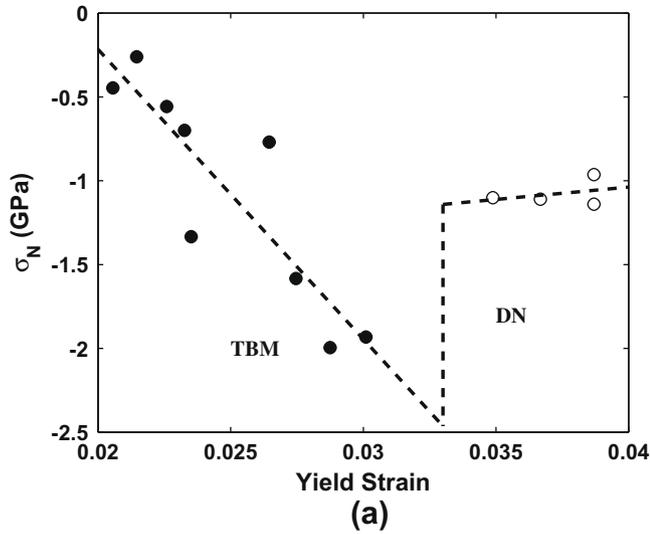
(a)

(b)

Fig. 4. (a) The normal stress, $\langle \sigma_N \rangle$, and (b) the critical resolved shear stress, $\langle \sigma_R \rangle$, plotted as a function of the yield strain for twinned copper nanopillars under compression. A clear bifurcation in the yield mechanisms takes place around a strain of 3.3%. The black dots indicate yielding by twin boundary migration and the white dots indicate yielding by dislocation nucleation.

boundaries is reduced whether the normal stress is tensile or compressive.

3.3. Atomistic deformation mechanism

Fig. 6 shows a time sequence of the deformation response of a characteristic simulation under compression. In order to eliminate thermal noise in the figure, the plotted atomic positions are taken as the mean positions over 10 ps. We have shown that twin boundary migration is a stick–slip mechanism [31], and, as such, once the initial migration event occurs at $t = 0.74$ ns it is quickly followed up by successive twin boundary migration events as a result of the nucleation and motion of twinning dislocations at $t = 0.76$ ns and $t = 0.78$ ns. Under tension, a similar behavior is also observed, as can be seen in Fig. 7. The reversibil-
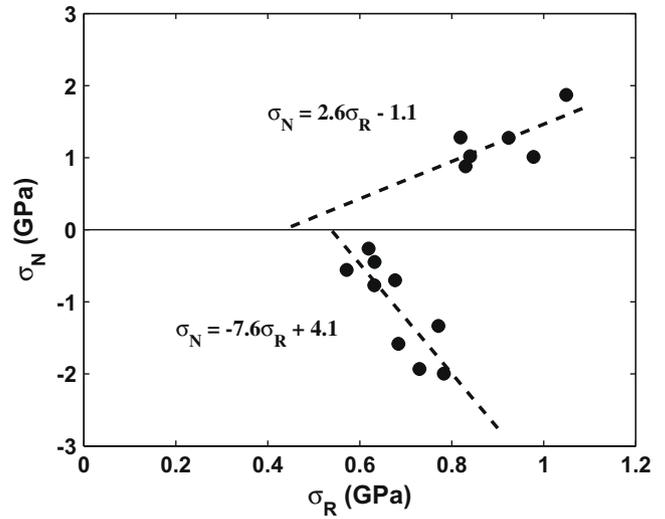

Fig. 5. Yield locus for reversible plasticity shown as the normal stress, $\langle \sigma_N \rangle$ plotted as a function of the critical resolved shear stress, $\langle \sigma_R \rangle$ for twinned nanopillars in tension (positive $\langle \sigma_N \rangle$) and in compression (negative $\langle \sigma_N \rangle$).

ity of twin boundary migration can be seen by comparing the nanopillar shape between the two figures, where the load axis shifts to the left under compression (Fig. 6),
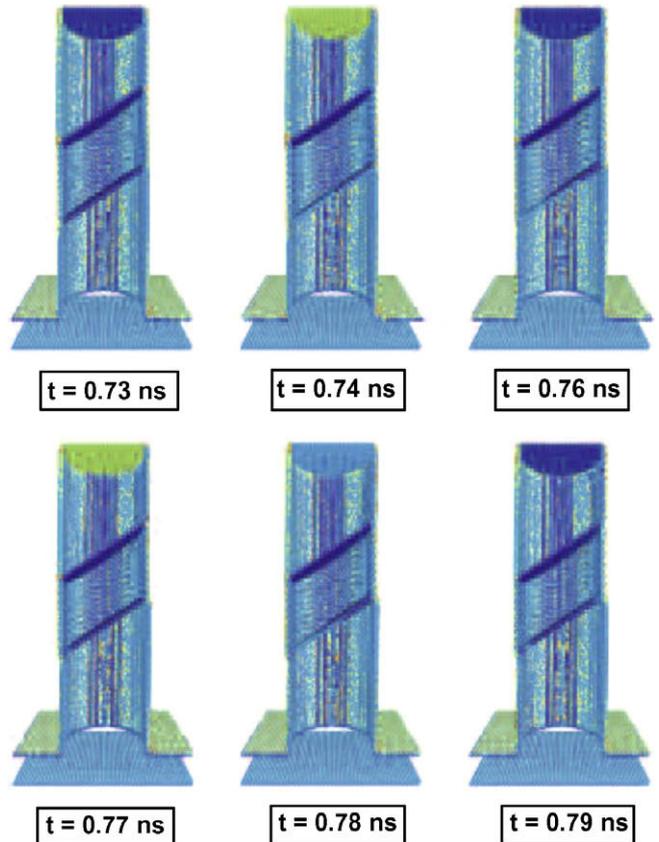

Fig. 6. Time sequence of the yielding of nanopillar compression at $\theta = 35.3°$. Atoms are labeled according to their centrosymmetry parameter. The front half of the nanopillar has been cut away for the purpose of this visualization in order to reveal the twinned nanostructure within. The atomic positions are averaged over 5000 time steps (10 ps) to remove noise due to thermal vibrations.

and to the right (Fig. 7) under tension. We note here that at strains larger than 3.3% ($t > 1.25$ ns in Fig. 7), a surface dislocation is emitted near the top of the pillar.

Hu et al. showed that the fundamental mechanism of twin boundary migration is the nucleation of a twinning partial dislocation at the twin boundary, and the corresponding motion of a Shockley partial dislocation across the twin interface resulting in a shift of the boundary plane either up or down [31]. Fig. 8 presents a detailed view of the basic twin boundary migration atomic mechanism leading to reversible plasticity by twin boundary migration. Atoms in the figure are highlighted according to their coordination number, and those with a coordination number of 12 are rendered invisible, thus eliminating bulk atoms as well as atoms comprising the twin plane from the visualization. Only the surface atoms and the atoms comprising the Shockley partial dislocation loop remain visible. The migration velocity of the Shockley partial dislocations responsible for twin boundary migration was calculated for selected cases of $\langle \sigma_N \rangle$. These results are presented in Table 1.

It is apparent from Table 1 that the speed of Shockley partials is significantly affected by the normal stress imposed on the twin boundary. At higher normal stress, either in tension or compression, Shockley partial dislocations move at slower speed. Pimpec [35] recently measured the speed of acoustic waves in copper, and determined that the velocity of the longitudinal wave $v_p = 4.76$ km s^{-1}, the

shear wave $v_s = 2.325$ km s^{-1} [36] and the Rayleigh wave $v_R = 2.16$ km s^{-1}. We find from the present simulations that the migration speed of Shockley partial dislocations sweeping across the twin plane is subsonic when there is either tension or compression acting on the twin boundary, and slightly supersonic when only shear is applied at the twin boundary. It is roughly $0.5v_s$ at a tensile stress of ≈ 2 GPa, and reaches v_s when σ_N is absent, consistent with the simulation results of Heino et al. [37]. Note that tension slows down Shockley partials more than compression does.

Fig. 8 shows a visualization of the propagation of Shockley partial dislocations, where a slice of the pillar isolating only a few planes above and below the twin plane is illustrated. Atomic positions are the result of averaging over 50 time steps (0.1 ps). At high values of the compressive stress component (left panel), the dislocation is identified as a $B\delta$ Shockley partial according to the Thompson notation, while the dislocation in the right panel under small compressive stress is $D\delta$. The dislocation loop, which nucleates from the intersection between the twin boundary and the free surface, is visibly slower at high values of compression.

4. Summary and conclusions

Plastic deformation of twinned copper nanopillars shows behavior that is not observed in the deformation of bulk copper. The unique features of this deformation stem from the small size and the ability to control the type and nature of dislocation nucleation and motion inside these nanosystems. While plastic deformation of bulk copper is controlled by dislocation multiplication and recovery processes, rather than by nucleation events, the situation in nanopillars is distinctly different. The present work shows that relatively simple placement of twin boundary orientation with respect to the load axis can give enough flexibility to control the stress state acting on individual twin or slip plans. This unique ability makes it possible to show a number of conclusions, as follows;

1. The yield locus for twinned copper nanopillars is an approximate linear relationship between the shear and normal components of the average atomic stress on twin planes. It is shown that, in tension, when $\sigma_N \approx 2$ GPa, and above ≈ 2.5 GPa in compression, plastic deformation is irreversible. Below these values, plasticity of twinned nanopillars is found to be reversible.
2. The critical transition from reversible to irreversible plasticity is shown to take place at a strain of $\approx 3.3\%$.
3. We show here that reversible plastic yield under tension is not the same as under compression, which indicates a clear "tension–compression asymmetry" in the reversible plasticity of twinned nanopillars.
4. The reversible–irreversible plasticity transition is found to be the result of a competition between the nucleation and growth of twinning dislocations favoring reversible
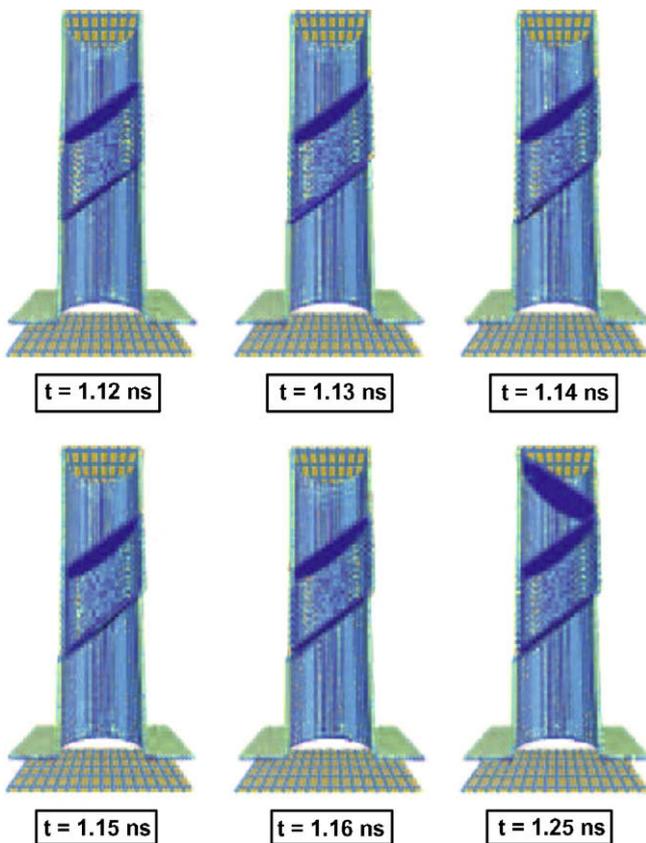

Fig. 7. Time sequence of the yielding of nanopillar tension at $\theta = 35.3°$. All other conditions are the same as in Fig. 6.
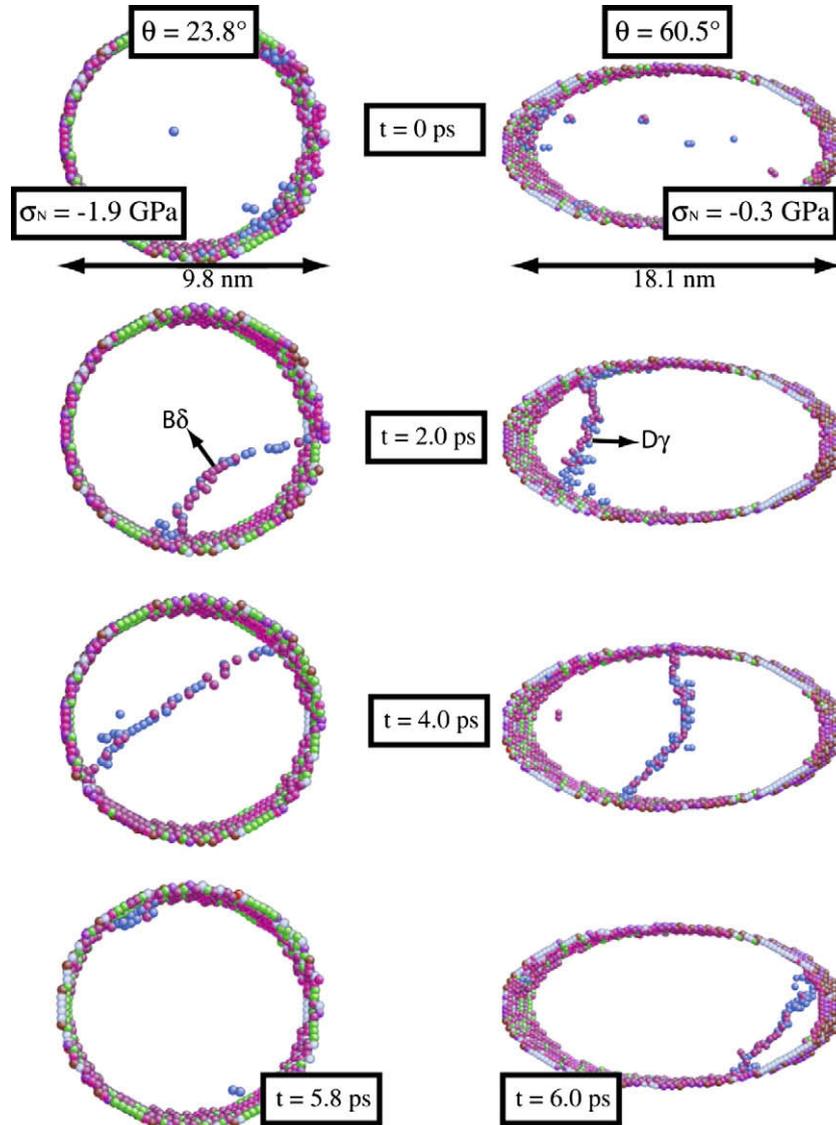
Fig. 8. Diagram showing the twin boundary migration mechanism for two characteristic compression simulations. Atoms are colored according to their coordination number, with those having 12 nearest neighbors removed. This visualization shows a slice of the pillar isolating only a few planes above and below the twin plane where the yielding event occurred. Atomic positions are the result of averaging over 50 time steps (0.1 ps)

Table 1
Twin boundary dislocation migration velocities for selected values of $\langle \sigma_N \rangle$ at the yield point and at $T = 500$ K. v/v_0 is the ratio of the migration velocity to the shear wave speed of 2.33 km s^{-1} [35,36], confirmed also by our MD simulations of non-twinned copper crystals.

	Tension			Compression		
$\langle \sigma_N \rangle$ (GPa)	1.9	1.3	0.9	−1.9	−0.7	−0.3
v (km/s)	1.3	2.1	2.6	1.6	1.9	2.4
v/v_0	0.56	0.89	1.06	0.70	0.81	1.04

plasticity on the one hand, vs. dislocation emission from free surfaces favoring irreversible plasticity on the other.
5. At higher normal stress (tension or compression), Shockley partial dislocations are slowed down. We find that the migration speed of Shockley partial dislocations sweeping across the twin plane is subsonic when there is either tension or compression acting on the twin boundary, and slightly supersonic when only shear is applied at the twin boundary.

Acknowledgements

References

[1] Boyko VS, Garber RI, Kossevich A. Reversible crystal plasticity. Woodbury, NY: American Institute of Physics; 1994.
[2] Lieber CM. MRS Bull 2003;28:486–91.
[3] Lu L, Shen Y, Chen X, Qian L, Lu K. Science 2004;304:422–6.
[4] Lu L, Schwaiger R, Shan ZW, Dao M, Lu K, Suresh S. Acta Mater 2005;53:2169–79.

[5] Ma E, Wang YM, Lu QH, Sui ML, Lu L, Lu K. Appl Phys Lett 2004;85:4932–4.

[6] Zhao WS, Tao NR, Guo JY, Lu QH, Lu K. Scripta Mater 2005;53:745–9.

[7] Xu D, Kwan WL, Chen K, Zhang X, Ozlino̅ V, Tu KN. Appl Phys Lett 2007;91:254105.

[8] Zhu T, Samanta A, Kim HG, Suresh S. Proc Natl Acad Sci 2007;104:3031.

[9] Horstemeyer MF, Baskes MI, Plimpton SJ. Acta Mater 2001;49(20):4363–74.

[10] Ostrom R, Tanenbaum D, Gallagher A. Appl Phys Lett 1992;61:925.

[11] Chen W, Ahmed H. Appl Phys Lett 1993;63:1116.

[12] Tada T, Kanayama T. J Vac Sci Technol B 1995;13:2801–4.

[13] Tada T, Kanayama T, Koga K, Weibel P, Carroll S, Seeger K, et al. J Phys D 1998;31:L21–4.

[14] Pedraza A, Fowlkes J, Lowndes D. Appl Phys Lett 1999;74:2322.

[15] Lewis P, Ahmed H, Sato T. J Vac Sci Technol B 1998;16(6):2938.

[16] Rabkin E, Nam HS, Srolovitz DJ. Acta Mater 2007;55:2085.

[17] Ma F, Ma SL, Xu KW, Chu PK. Nanotechnology 2007;18:455702.

[18] Zhu T, Li J, Samanta A, Leach A, Gall K. Phys Rev Lett 2008;100:025502.

[19] Cao A, Ma E. Acta Mater 2008;56:4618–828.

[20] Zepeda-Ruiz LA, Sadigh B, Diener J, Hodge AM, Hamza AV. Appl Phys Lett 2007;91:101907.

[21] Gall K, Diao J, Dunn ML. Nano Lett 2004;4:2431.

[22] Afanasyev KA, Sansoz F. Nano Lett 2007;7:2056.

[23] Park HS, Zimmerman JA. Phys Rev B 2005;72:054106.

[24] Diao J, Gall K, Dunn ML, Zimmerman JA. Acta Mater 2006;54:643.

[25] Li L, Ghoniem N. Phys Rev B 2008;79(7):075444.

[26] Tschopp MA, McDowell DL. J Mech Phys Solids 2008;56:1806–30.

[27] Dutta A, Bhattacharya M, Barat P, Mukherjee P, Gayathri N, Das GC. Phys Rev Lett 2008;101:115506.

[28] Mishin Y, Mehl MJ, Papaconstantopoulos DA, Voter AF, Kress JD. Phys Rev B 2001;63:224106.

[29] Ackland GJ, Finnis MW. Phil Mag A 1986;54:301.

[30] Gumbsch P, Daw MS. Phys Rev B 1991;44:3934.

[31] Hu Q, Li L, Ghoniem NM. Acta Mater 2009;57(16):4866–73.

[32] Mishin Y, Suzuki A, Uberuaga BP, Voter AF. Phys Rev B 2007;75:224101.

[33] Cahn JW, Mishin Y, Suzuki A. Acta Mater 2006;54:4953–75.

[34] Brown JA, Ghoniem NM. Acta Mater 2009;57(15):4454–62.

[35] Pimpec FL. Limitations on the use of acoustic sensors in rf breakdown localization. Technical Report SLAC-TN-04-049 LCC-0149, SLAC National Accelerator Laboratory; 2008.

[36] Lide DR, editor. Handbook of chemistry and physics. Boca Raton, FL: CRC Press; 1994.

[37] Heino P, Ristolainn E. NanoStruct Mater 1999;11(5):587–94.